Materials Science and Technology (MS&T) 2007
September 16-20, 2007, Detroit, Michigan · Copyright © 2007 MS&T'07®
FUNDAMENTALS AND CHARACTERIZATION: Numerical, Mathematical and Physical Modeling Tools for Materials Processes
Organized by Patricio F. Mendez and Ben Q. Li
Numerical, Mathematical, and Physical Modeling Tools for Materials Processes III

A Numerical Study of Plasma-Particle Energy Exchange Dynamics in Induction Thermal Plasmas for Glassification

M. M. Hossain, Y. Yao and T. Watanabe

Department of Environmental Chemistry and Engineering
Tokyo Institute of Technology, G1-22, 4259 Nagatsuta, Yokohama 226-8502, Japan

Abstract

Dependence of energy exchange between plasma and soda-lime-silica glass particles on the particle size, powder feed-rate and nozzle insertion length during in-flight thermal treatment for glassification by induction thermal plasmas has been studied. For the numerical investigation into the plasma-particle energy exchange dynamics during melting and vaporization of particles, a thermofluid plasma-particle interaction model has been developed taking into account the strong plasma-particle interactions and particle loading effects. It is found that heat transfer to the particles depends strongly on the particles size, powder feed-rate, nozzle insertion length, and plasma discharge parameters. Thus, for the efficient thermal treatment of particles, the above parameters should be optimized.

Keywords: Plasma-particle interaction, Energy transfer, Soda-lime-silica glass.

Introduction

Thermal plasma processing has become indispensable in a wide variety of disciplines from nano-materials synthesis to surface treatment of ceramic micro-particles [1-2]. Besides the experimental diagnosis, numerical analysis is important in the research and development of the thermal plasma technologies. After in-flight thermal treatment of particles, the diagnoses of experimental products usually provide information on the final characteristics of the particles. On the other hand, numerical analysis provides insight on the thermal histories of the particles during in-flight treatment. It is our aim to melt and modify the size, morphology, and composition of granulated sola-lime-silica glass particles by in-flight treatment in an induction thermal plasma reactor. The modeling of particle heating in induction plasmas has been pioneered by Yoshida *et al* [3] and Boulos [4] among others. Later Proulx *et al* [5] discussed the particle loading effects taking into account the plasma-particle interaction effects for alumina and copper particles in argon plasmas. In the present work, mathematical modeling of plasma-particle interaction and energy exchange during in-flight melting and vaporization of soda-lime-silica glass particles in argon–oxygen induction thermal plasmas is performed under LTE (local thermodynamic equilibrium) and laminar plasma flow conditions. The objective of this study is to investigate the particle surface treatment in induction thermal plasmas, with emphasis on the impacts of feed particle size, powder feed-rate and nozzle insertion length on the plasma–particle energy exchange. The effects of above parameters on plasma-particle energy exchange and further consequences will be discussed in detail.

Modeling

Plasma Model

Fig.1 shows the schematic geometry of the torch used in the modeling of plasma-particle interaction and flow. Torch dimensions and plasma discharge conditions are tabulated in Table 1. The torch consists of water cooled coaxial quartz tube, surrounded by 3-turn induction coil. Soda-lime-silica glass powders premixed with carrier gas are injected into the plasma torch through the nozzle tube inserted into the high temperature region of the plasma torch. The working gases are argon and oxygen. In this model, it is assumed that plasma is in LTE (local thermodynamic equilibrium) condition, and optically thin; plasma flow is 2-dimensional, axi-symmetric, and laminar. Electromagnetic fields are assumed to be 2-dimensional. In this model, the conservation equations are as follows:

Mass conservation:

$$\nabla \cdot \rho \mathbf{u} = S_p^C \qquad (1)$$

Momentum conservation:

$$\rho \mathbf{u} \cdot \nabla \mathbf{u} = -\nabla p + \nabla \cdot \mu \nabla \mathbf{u} + \mathbf{J} \times \mathbf{B} + S_p^M \qquad (2)$$

Energy conservation:

$$\rho \mathbf{u} \cdot \nabla h = \nabla \cdot \left(\frac{\kappa}{C_p} \nabla h \right) + \mathbf{J} \cdot \mathbf{E} - Q_r + S_p^E \qquad (3)$$

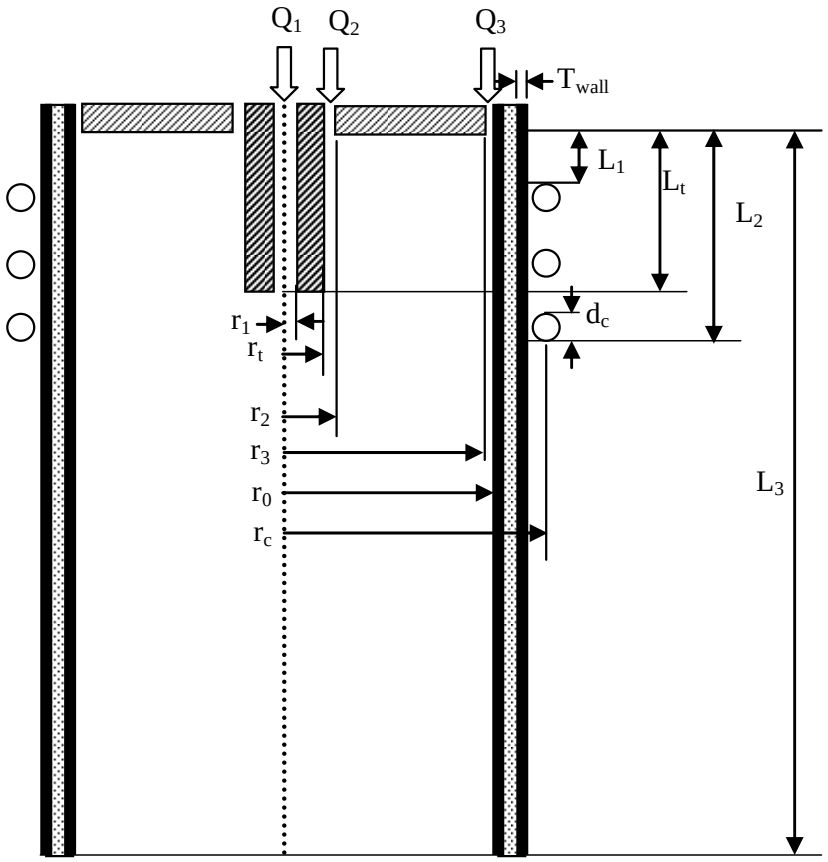

Fig.1 Schematic geometry and dimensions of ITP torch

Table 1 Torch dimensions and discharge conditions

Distance to initial coil position (L_1)	19 mm
Distance to end of coil position (L_2)	65 mm
Torch length (L_3)	190 mm
Length of injection tube (L_t)	52 mm
Coil diameter (d_c)	5 mm
Wall thickness of quartz tube (T_{wall})	1.5 mm
Inner radius of injection tube (r_1)	1 mm
Outer radius of injection tube (r_t)	4.5 mm
Outer radius of inner slot (r_2)	6.5 mm
Inner radius of outer slot (r_3)	21.5 mm
Torch radius (r_0)	22.5 mm
Coil radius (r_c)	32 mm
Plasma power	10 kW
Working frequency	4 MHz
Working pressure	0.1 MPa
Flow rate of carrier gas (Q_1)	4 ~ 9 lpm of Argon
Flow rate of plasma gas (Q_2)	2 lpm of Argon
Flow rate of sheath gas (Q_3)	22 lpm Argon & 2 lpm Oxygen

Species conservation:

$$\rho \mathbf{u} \cdot \nabla y = \nabla \cdot \left(\rho D_m \nabla y \right) + S_p^C \qquad (4)$$

Vector potential form of Maxwell field equation [6]:

$$\nabla^2 \mathrm{A_c} = i \mu_0 \sigma \omega \mathrm{A_c} \qquad (5)$$

Where, ∇: vector operator, **u**: velocity vector, ρ: mass density, μ: viscosity, σ: electrical conductivity, κ: thermal conductivity, h: enthalpy, p: pressure, C_p: specific heat at constant pressure, D_m: multicomponent diffusion coefficient, y: mass fraction, **J**: current density vector, **E**: electric field vector, **B**: magnetic field vector, Q_r: volumetric radiation loss, $\mathrm{A_c}$: complex amplitude of vector potential, μ_0: permeability of free space, ω: $2\pi f$ (f: frequency), i: complex vector ($\sqrt{-1}$). The particle source terms S_p^C, S_p^M and S_p^E are the contributions of particles to the mass and species, momentum and energy conservation equations respectively.

The boundary conditions, thermodynamic and transport properties of argon and oxygen gases and calculation procedure are the same as those described in our previous work [7].

Particle Model

The following assumptions are made in the analysis of plasma-particle interactions; the particle motion is two-dimensional, only the viscous drag force and gravity affect the motion of an injected particle, the temperature gradient inside the particle is neglected, and the particle charging effect caused by the impacts of electrons or positive ions is negligible. The electromagnetic drag forces caused by the particle charging of the injected powder are negligible compared with those by neutrals and charged particles due to negligible electrical conductivity of soda-lime powders. Thus, the momentum equations for a single spherical particle injected vertically downward into the plasma torch can be expressed as follows:

$$\frac{du_p}{dt} = -\frac{3}{4} C_D (u_p - u) U_R \left(\frac{\rho}{\rho_p d_p} \right) + g \quad (6)$$

$$\frac{dv_p}{dt} = -\frac{3}{4} C_D (v_p - v) U_R \left(\frac{\rho}{\rho_p d_p} \right) \quad (7)$$

$$U_R = \sqrt{(u_p - u)^2 + (v_p - v)^2} \quad (8)$$

The particle temperature, liquid fraction and diameter are predicted according to the following energy balances:

$$Q = \pi d_p^2 h_c \left(T - T_p \right) - \pi d_p^2 \sigma_s \varepsilon \left(T_p^4 - T_a^4 \right) \quad (9)$$

$$\frac{dT_p}{dt} = \frac{6Q}{\pi \rho_p d_p{}^3 C_{pp}}, \quad T_p < T_b \quad (10)$$

$$\frac{dx}{dt} = \frac{6Q}{\pi \rho_p d_p{}^3 H_m}, \; 1000 \le T_\mathrm{p} \le 1600 \quad (11)$$

$$\frac{dd_p}{dt} = -\frac{2Q}{\pi \rho_p d_p{}^2 H_v}, \; 1000 \le T_\mathrm{p} \le 1600, \; T_p \ge T_b \quad (12)$$

where u_p: axial velocity component of particle, $v_{p:}$ radial velocity component of particle, g: acceleration of gravity, ρ_p: particle mass density, d_p: particle diameter, Q: the net heat exchange between the particles and its surroundings, T_p, T_m and T_b: particle temperature, melting point temperature and boiling point temperature, respectively, T: plasma temperature, T_a: ambient temperature, ε: particle surface emissivity; σ_s: Stefan-Boltzmann constant, C_{pp}: particle specific heat, H_m and H_v: latent heat of particle melting and vaporization respectively, and x: the liquid mass fraction of the particle.

Drag coefficient C_{Df} is calculated using equation (13) and the property variation at the particle surface layer and the non-continuum effects are taken into account by equation (14) and (15) [8].

$$C_{D\mathrm{f}} = \begin{cases} \dfrac{24}{R_e} & R_e \le 0.2 \\ \dfrac{24}{R_e}\left(1 + \dfrac{3}{16} R_e\right) & 0.2 < R_e \le 2.0 \\ \dfrac{24}{R_e}\left(1 + 0.11 R_e{}^{0.81}\right) & 2.0 < R_e \le 21.0 \\ \dfrac{24}{R_e}\left(1 + 0.189 R_e{}^{0.62}\right) & 21.0 < R_e \le 200 \end{cases} \quad (13)$$

$$f_1 = \left(\frac{\rho_\infty \mu_\infty}{\rho_s \mu_s} \right)^{-0.45} \quad (14)$$

$$f_2 = \left\{ 1 + \left(\frac{2-\alpha}{\alpha} \right) \left(\frac{\gamma}{1+\gamma} \right) \frac{4}{Pr_s} Kn \right\}^{-0.45}, 10^{-2} < Kn < 1 \quad (15)$$

$$C_D = C_{Df} f_1 f_2 \quad (16)$$

To take into account the steep temperature gradient between plasma and particle surface, the Nusselt correlation can be expressed by equation (17) [9]. The non-continuum effect is taken into account by equation (18) [8].

$$Nu_f = (2.0 + 0.6 R_{ef}^{1/2} Pr_f^{1/3}) \left(\frac{\rho_\infty \mu_\infty}{\rho_s \mu_s} \right)^{0.6} \left(\frac{C_{p\infty}}{C_{ps}} \right)^{0.38} \quad (17)$$

$$f_3 = \left\{ 1 + \left(\frac{2-\alpha}{\alpha} \right) \left(\frac{\gamma}{1+\gamma} \right) \frac{4}{Pr_s} Kn \right\}^{-1}, \ 10^{-3} < Kn < 1 \quad (18)$$

The convective heat transfer coefficient is predicted as follows:

$$h_{cf} = \frac{\kappa_f}{d_p} Nu_f f_3 \quad (19)$$

In the above expressions, subscript f, ∞ and s refer to properties corresponding to the film temperature (arithmetic mean of plasma and particle temperatures), plasma temperature and particle temperature respectively, C_{pp}: particle specific heat, ρ_p: particle mass density, h_c: heat transfer coefficient, *Nu*: Nusselt number, *Pr*: Prandtl number, *Re*: Reynold number, $\propto$: thermal accommodation coefficient, γ: specific heat ratio and *Kn*: Knudsen number. The physical properties of soda-lime glass powders are: mass density 2300 kg/m^3, specific heat 800 J/kg-K, surface emissivity 80%, fusion and boiling temperature 1000~1600 K and 2500 K respectively, heat of fusion, and vaporization 3.69×10^5 J/kg and 1.248×10^7 J/kg, respectively.

Particle Source Terms

For the sake of computation, the particle concentration in the inlet is assumed to be uniform and to be separated into five injection points, which are at radial positions of 0.3, 0.45, 0.6, 0.75 and 0.9 mm. In the present computation, powder diameter distributions are assumed to be very close to Maxwellian distribution. There are seven diameters of particles and the average powder diameter is 58 μm with the maximum deviation of 67%. As a result, that gives rise to 35 different possible particle trajectories. The injection velocity of the particles is assumed to be equal to the initial velocity of carrier gas. To take into account the particle loading effects the particle source terms for the mass, momentum, energy and species conservation equations have been calculated in the same fashion as described in Ref. [5] using the Particle-Source-In Cell

(PSI-CELL) approach [10] where the particles are regarded as sources of mass, momentum and energy.

Results and Discussion

The torch dimensions and discharge conditions are tabulated in Table 1. After having the conversed plasma temperature and velocity with zero powder feed-rate, particle trajectories, velocity and temperature histories as well as the particle source terms are calculated with certain feed-rate. Incorporating the particle source terms, and recalculations of plasma fields are carried out. With the new plasma fields again the particle temperature, velocity, trajectories, and particle source terms are calculated. This process is repeated until convergence. The melting and reaction mechanisms in soda-lime-silica glass powders and the plasma-particle energy exchange phenomena are very complex. In this paper we shall discuss the impacts of particle size, powder feed-rate and nozzle insertion length on the plasma-particle energy exchange.

Impacts of Particle Size

Fig.2 shows the axial velocity distributions of plasma (at r=0) and particles along the trajectory, for a carrier gas flow-rate of 6 lpm and powder feed-rate of 5 g/min. It is found that initially the velocity of small particles (diameter: 20 μm) is higher than that of large particles (diameter: 90 μm). This is because, lighter initial momentum of small particles. But at the downstream of the torch the large particles attain higher velocity than that of small particles. It should be mentioned here that the velocity of small particle follows the same trend of plasma velocity. From this figure it is comprehended that in the high temperature plasma flame, the residence time of small particles is comparatively longer (6.14 ms) than that of large particles (5.98 ms). Fig.3 shows the energy transfer to particles for the same conditions of Fig.2. This figure clearly indicates that the energy transfer per particle sharply increases with the increase of

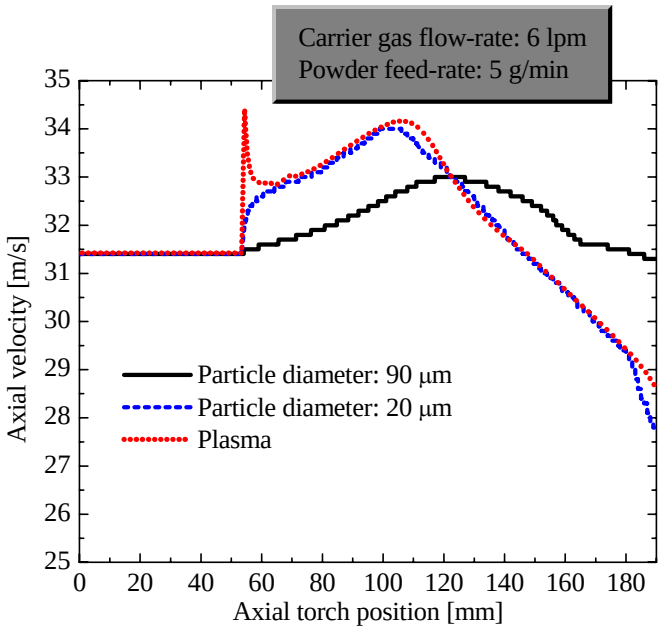

Fig.2 Axial velocity distributions of plasma (at r=0) and particles

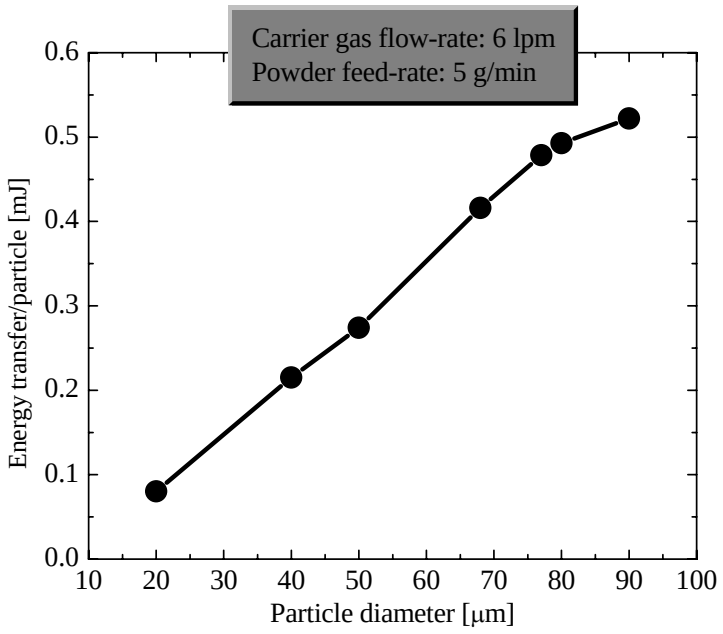

Fig.3 Dependence of energy transfer per particle on particle diameter

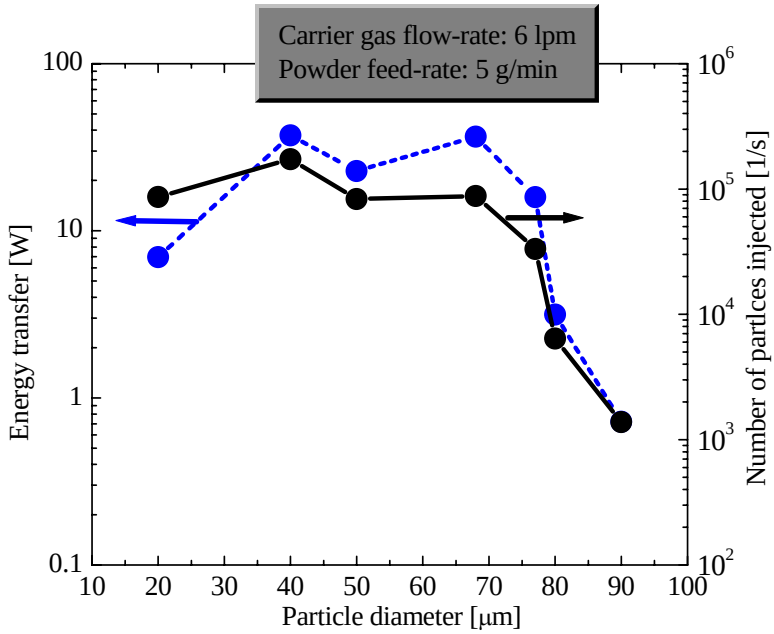

Fig.4 Dependence of energy transfer to particles on particle diameter

particle diameter. The probable reason is the large surface area of large particle than that of small particle. Fig.4 describes particle diameter dependence of energy transfer rate to particles. It can be noticed that energy transfer rate is governed strongly by the particle size distribution which attributed to the number of particles injected per unit time. As a result, energy transfer rate to small particles (20 μm) is higher than that of large particles (90 μm).

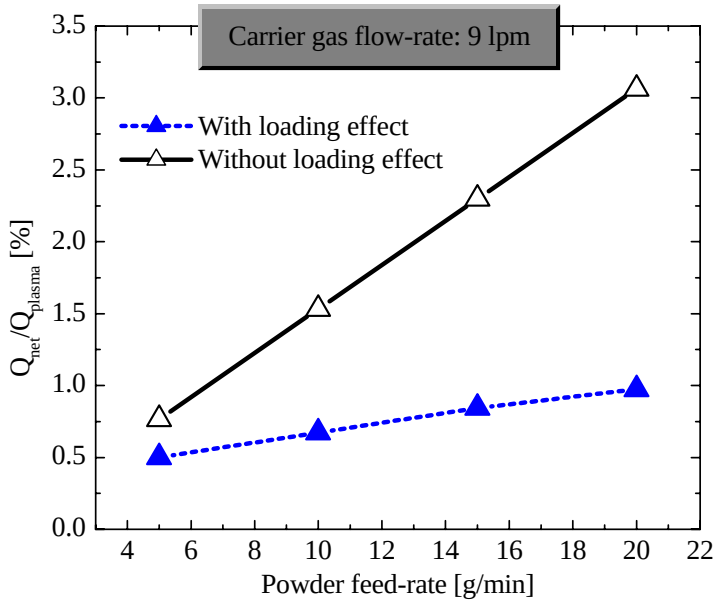

Fig.5 Effects of powder loading on energy transfer to particles

Impacts of Powder Feed-rate

It is found that powder feed-rate has strong influence on the energy transfer to particles. Fig.5 shows the percentage of plasma energy (Q_{plasma} = 10 kW) transferred to the particles with and without powder loading effects for a carrier gas flow-rate of 9 lpm. The net energy transfer to particles is calculated by integrating the energy transfer rate to each particle over the residence time for all the particle trajectories. Mathematically the net energy transfer to particles (Q_{net}) can be expressed as follows:

$$Q_t = \int_{t=0}^{t=t_s} \left\{ \pi d_p^2 h_c \left(T - T_p\right) - \pi d_p^2 \sigma_s \varepsilon \left(T_p^4 - T_a^4\right) \right\} dt \qquad (20)$$

$$Q_{net} = \sum_l \sum_k N^{(l,k)} Q_t \qquad (21)$$

Where, t_s is the residence time of particle in the plasma, l and k are the number of particle size and number of injection points respectively. Other variables are introduced in the particle model section. Usually without loading effects energy transfer increases linearly with feed-rate. When powder loading is taken into account, the energy transfer to particles still increases with feed-rate but with a declined slope. This phenomenon can be explained as follows. Energy transfer to particles is governed mainly by the plasma temperature. It is found that at a feed-rate of 15 g/min plasma temperature drops by 37% at the torch exit. Due to the significant cooling of plasma around the torch centerline at higher powder feed-rate, the energy transfer to particles decreases consequently.

Impacts of Nozzle Insertion Length

The energy transfer to injected particles has a strong dependence on the insertion length of the nozzle through which carrier gas and powders are injected into the plasma torch. As there is a strong vortex in the upper part of the torch, so it is difficult to inject carrier gas and powders without a nozzle inserted up to certain depth. Moreover, in case of powder feeding without

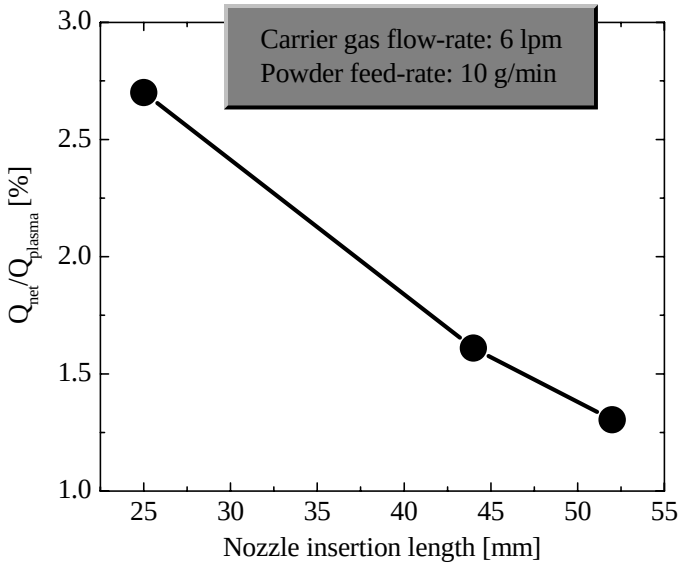

Fig.6 Effects of nozzle insertion length on energy transfer to particles

nozzle, particles (particularly small particles) can not penetrate the hot core of plasma [4]. In our experiment the insertion length was 52 mm from the top of the torch. As a result, a large portion of the hot plasma remains unused. Thus we examined the impacts of nozzle insertion length on the plasma-particle energy exchange. Fig.6 shows the dependence of energy transfer to particles on the nozzle insertion length. It is noticed that the percentage of energy transfer decreases with the increase of insertion length. The main reason is that with larger insertion length, the unused portion of high temperature plasma flame increases. In addition to that, the total flight time of particles in plasma contact decreases with longer insertion length. Thus for the maximum energy transfer efficiency, the nozzle insertion length should be as short as possible.

Conclusions

Simulated results show strong dependence of energy transfer to particles on particles size, powder feed-rate and nozzle insertion length. The predicted results reveal that energy transfer to particles is affected to a large extent by the particle diameter distributions. Higher powder feed-rate causes severe cooling of plasma around the torch centerline and thus declines the energy transfer to particle, which accordingly degrades the particle treatment quality. For the efficient use of plasma energy, the nozzle insertion length should be as short as possible. The simulated results lead to a better understanding of the powder treatment process in induction thermal plasmas, and consequently will be helpful to optimize the plasma and particle parameters for the efficient thermal treatment of particulate materials.

Acknowledgement

The financial support provided by JSPS (Japan Society for the Promotion of Science) is gratefully acknowledged.

References

[1] P. R. Taylor and S. A Pirzada, Thermal Plasma Processing of materials: A Review, *Advance Performance Materials*, Vol 1, 1994, p 35-50.
[2] T. Watanabe and K. Fujiwara, Nucleation and growth of oxide nanoparticles prepared by induction thermal plasmas, *Chem. Eng. Comm*., Vol 191, 2004, p 1343-1361.
[3] T. Yoshida and K. Akashi, Particle heating in radio-frequency plasma torch, *J. Appl. Phys.*, Vol 48, 1977, p 2252-2260.
[4] M. I. Boulos, Heating of powders in the fire ball of an induction plasma, *IEEE Trans. on Plasma Sci.*, Vol PS-6, 1978, p 93-106.
[5] P. Proulx, J. Mostaghimi and M. I Boulos, Plasma-particle interaction effects in induction plasma modeling under dense loading conditions, *Int. J. Heat Mass Transfer*, Vol 28, 1985, p 1327-1336.
[6] J. Mostaghimi, K. C Paul and T. Sakuta, Transient response of the radio frequency inductively coupled plasma to a sudden change in power, *J. Appl. Phys.*, Vol 83, 1998, p 1898-1908.
[7] M. M. Hossain, Y. Yao, Y. Oyamatsu, T. Watanabe, F. Funabiki and T. Yano, Determination of Melting Mechanism of Granular Powders for Vitrification by Argon-Oxygen Induction Thermal Plasmas, *WSEAS Trans. Heat and Mass Transfer*, Vol 1, 2006, p 625-631.
[8] X. Chen and E. Pfender, Effect of the Knudsen Number on Heat Transfer to a Particle Immersed into a Thermal Plasma, *Plasma Chem. Plasma Process*., Vol 3, 1983, p 97-113.
[9] Y. C. Lee, Y. P. Chyou, and E. Pfender, Particle Dynamics and Particle Heat and Mass Transfer in Thermal Plasmas. Part II. Particle Heat and Mass Transfer in Thermal Plasmas, *Plasma Chem. Plasma Process.,* Vol 5, 1985, p 391-414.
[10] C. T Crowe, M. P Sharma and D. E Stock, The Particle-Source-In Cell (PSI-CELL) Model for Gas-droplet Flows, *J. Fluid Eng.*, Vol 99, 1977, p 325-332.